Excitons Dominate the Emission from PM6:Y6 Solar Cells, but This Does Not Help the Open-Circuit Voltage of the Device

Peer-reviewed author version

Perdigon-Toro, Lorena; Phuong, Le Quang; Zeiske, Stefan; VANDEWAL, Koen; Armin, Ardalan; Shoaee, Safa & Neher, Dieter (2021) Excitons Dominate the Emission from PM6:Y6 Solar Cells, but This Does Not Help the Open-Circuit Voltage of the Device. In: ACS Energy Letters, 6 (2) , p. 557 -564.

DOI: 10.1021/acsenergylett.0c02572
Handle: http://hdl.handle.net/1942/33888

Excitons dominate the emission from PM6:Y6 solar cells but this does not help the open-circuit voltage of the device

*Lorena Perdigón-Toro[1,2], Le Quang Phuong[2], Stefan Zeiske[3], Koen Vandewal[4], Ardalan Armin[3], Safa Shoaee[2], Dieter Neher[1]**

[1]Soft Matter Physics and Optoelectronics, Institute of Physics and Astronomy, University of Potsdam, Karl-Liebknecht-Str. 24-25, 14476 Potsdam-Golm, Germany

[2]Optoelectronics of Disordered Semiconductors, Institute of Physics and Astronomy, University of Potsdam, Karl-Liebknecht-Str. 24-25, 14476 Potsdam-Golm, Germany

[3]Sustainable Advanced Materials (Sêr SAM), Department of Physics, Swansea University, Singleton Park, Swansea, SA2 8PP U.K.

[4]Instituut voor Materiaalonderzoek (IMO-IMOMEC), Hasselt University, Wetenschapspark 1, BE-3590 Diepenbeek, Belgium

email: neher@uni-potsdam.de

Abstract

Non-fullerene acceptors (NFAs) are far more emissive than their fullerene-based counterparts. Here, we study the spectral properties of photocurrent generation and recombination of the blend of the donor polymer PM6 with the NFA Y6. We find that the radiative recombination of free charges is almost entirely due to the re-occupation and decay of Y6 singlet excitons, but that this pathway contributes less than 1 % to the total recombination. As such, the open-circuit voltage of the PM6:Y6 blend is determined by the energetics and kinetics of the charge transfer state. Moreover, we find that no information on the energetics of the CT state manifold can be gained from the low energy tail of the photovoltaic external quantum efficiency spectrum, which is dominated by the excitation spectrum of the Y6 exciton. We, finally, estimate the charge separated state to lie only 120 meV below the Y6 singlet exciton energy, meaning that this blend indeed represents a high efficiency system with a low energetic offset.

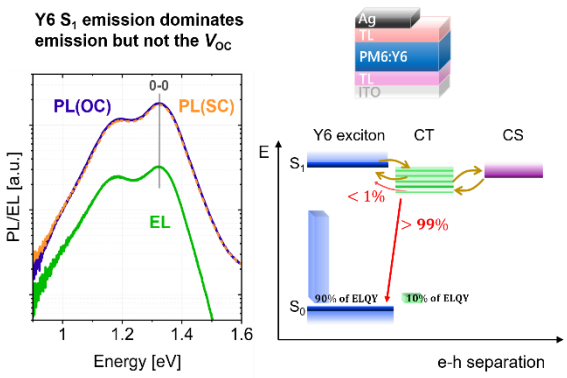

State-of-the-art power conversion efficiencies (PCE) of organic solar cells (OSCs) are now above 18 % (certified 17.4 %),[1] largely due to the introduction of non-fullerene acceptors, NFAs, replacing formerly used fullerene derivatives such as PCBM or ICBA. OSCs based on NFAs nowadays approach their inorganic competitors in terms of photocurrent production and external quantum efficiencies (EQE), owing to their strong and complementary absorption, but lag behind with regards to their open-circuit voltage (V_{OC}).[2] However, compared to fullerene-devices, NFA-based solar cells generally exhibit lower non-radiative V_{OC} losses,[3] as a result of a higher radiative efficiency of free carrier recombination. There are indeed important features that set NFAs apart from fullerenes. First, in contrast to C_{60} and its soluble derivatives, the lowest excited state of NFAs is a singlet exciton and NFA layers with reasonably high photoluminescence quantum efficiencies, in the 0.1 to 10 % range, have been reported.[4,5] Second, NFAs usually have a planar conjugated backbone, allowing face to face pi-stacking with each other and the donor molecules.[6,7] DFT calculations indeed predict significant electronic coupling between the NFA and the donor molecules.[7] This has been proposed to result in an intensity borrowing mechanism for optical transitions from the interfacial charge transfer (CT) state, hereby increasing the radiative decay efficiency.[8,9] More recently, it was proposed that the increased radiative decay efficiency results from the fact that the occupation of the singlet excitons is in equilibrium with the CT population.[10]

The blend of the donor polymer PM6 with the NFA acceptor Y6 has become the *fruit fly* of research on NFA-based solar cells (see **Figure 1a** for the chemical structures). This is because of the high efficiency (>15 %) of single junction PM6:Y6 solar cells, which has now been reproducibly achieved in many labs around the world. The high short-circuit current (J_{SC}) is a consequence of efficient light absorption over a wide spectral range (see **Figure 1b**) in combination with field-independent photocurrent generation.[11] On the other hand, reported V_{OC} values range from 0.82-0.85 eV, which is much smaller than the photovoltaic gap E_G of the blend of around 1.38 eV (see **Figure S1**). Detailed understanding of the processes causing this significant voltage loss requires knowledge about the energies and decay properties of the excited states involved in the process of free charge generation and recombination. However, the deconvolution of the device absorption and emission spectra into contributions from the CT and singlet states has turned out to be difficult; where in particular the reported values for the CT energy, E_{CT}, vary significantly in the literature.[12–14] Similarly to other high performance NFA-based blends, this is in part due to the much higher oscillator strength of the NFA singlet (S_1) excited state compared to the CT state, combined with a (desired) small S_1-CT energy offset. Moreover, microcavity effects play a role in altering the spectral shape of the emission spectrum of a complete device.[15–17] Given that those microcavity effects depend strongly on the optical properties of the film which itself depends on the layer composition, the often used approach to distinguish the spectral signatures of singlet and CT states by comparing the

electroluminescence spectra of the neat NFA and of the donor:NFA blend may not be appropriate.

Here, we present the results of a careful analysis of the photoluminescence (PL) and electroluminescence (EL) spectra of PM6:Y6 blends in different sample geometries. We show that the external EL of the device is almost entirely determined by the re-occupation of the Y6 singlet. Despite this, less than 1 % of the recombination proceeds through the S_1 state and free charges recombine almost entirely through a state manifold which has a maximum radiative efficiency of $4x10^{-6}$, and which we tentatively assign to the CT state manifold. We also show that absorption from S_1 completely dominates the photovoltaic external quantum efficiency, EQE_{PV}, and that no information on the energetics of the CT state manifold can be gained from the low energy EQE_{PV} tails. By comparing temperature dependent PL of Y6 and temperature dependent EL of PM6:Y6, we finally estimate the charge separated (CS) state to lie only 120 meV below the singlet energy, E_{S1}, meaning that this blend indeed represents a high efficiency system with a low energetic offset.

Figure 1a shows the current density-voltage (*JV*) curve of a regular PM6:Y6 bulk heterojunction (BHJ) device with an active layer thickness of 100 nm (see **Table S1** and **Figure S2** for the *JV* parameters and characteristics of the blend in other device configurations). The device has a V_{OC} of 0.84 V, which means that the quasi-Fermi level splitting is significantly smaller than the energy of the absorption onset. Convoluting EQE_{PV} with the black body photon flux allows calculation of a radiative upper limit,[18] $V_{OC,rad}$ of 1.08 V, ca. 0.30 eV below the photovoltaic bandgap of 1.38 eV yet, 0.24 V larger than the measured V_{OC} (see **Table S2** in the Supporting Information). The latter additional voltage loss, $\Delta V_{\mathrm{OC,nrad}}$, originates from non-radiative recombination and is related to the external quantum efficiency of electroluminescence, ELQY, via $q\Delta V_{\mathrm{OC,nrad}} = k_B T \ln(\mathrm{ELQY})$, with q being the elementary charge, k_B the Boltzmann constant and T the absolute temperature of the device. For our regular device, we measure $\mathrm{ELQY} = 2.7x10^{-5}$, yielding $\Delta V_{\mathrm{OC,nrad}} = 0.27\,\mathrm{eV}$, in good agreement with the difference between $V_{OC,rad}$ and the measured V_{OC} of 0.24 eV. Importantly, this $\Delta V_{\mathrm{OC,nrad}}$ is about 0.1 V lower as compared to most fullerene-based devices.[19,20] As discussed earlier, this has been attributed to the high oscillator strength of the local exciton (LE) on the NFA, which increases the ELQY via e.g., LE-CT hybridization or by repopulation of the Y6 singlet exciton from the CT state. In the following, we will argue that exciton reformation indeed dominates the radiative recombination of free charges in this blend, but that this process has no beneficial effect on the V_{OC} of the device.

Figure 1c and **Figure 1d** compare the PL spectra of thin films of neat Y6, a 1:1.2 (wt.%) PM6:Y6 BHJ blend and a 1:1.2 (wt.%) blend of Y6 with the inert polymer polystyrene (PS) on glass substrates. We measure external photoluminescence quantum efficiencies (PLQY) of $7x10^{-3}$ in both the neat Y6 and the PS:Y6 blend, while the PM6:Y6 has a significantly smaller PLQY of $3.1x10^{-4}$ indicating efficient exciton dissociation with subsequent non-radiative decay.

These measurements were done in a way that they determine the external PL efficiency, i.e. the PL efficiency for photons coupled out of the thin film (see experimental section in the Supporting Information). The shape of the PL spectrum is similar for all three films, with a maximum at around 1.3 eV and a shoulder at ca. 1.2 eV, which we assign to the 0-0 transition and 0-1 transitions in the vibronic progression of Y6.[21] There are, however, differences in the emission energies and relative strengths already between the neat Y6 film and the PS:Y6 blend, and more prominently when compared to PM6:Y6. Besides being due to donor-acceptor interactions, these changes might be due a slightly different packing and orientation of Y6 in the different samples. Such spectral changes are expected to become even more prominent in the EL spectra of the corresponding devices due to microcavity effects.[16,17]

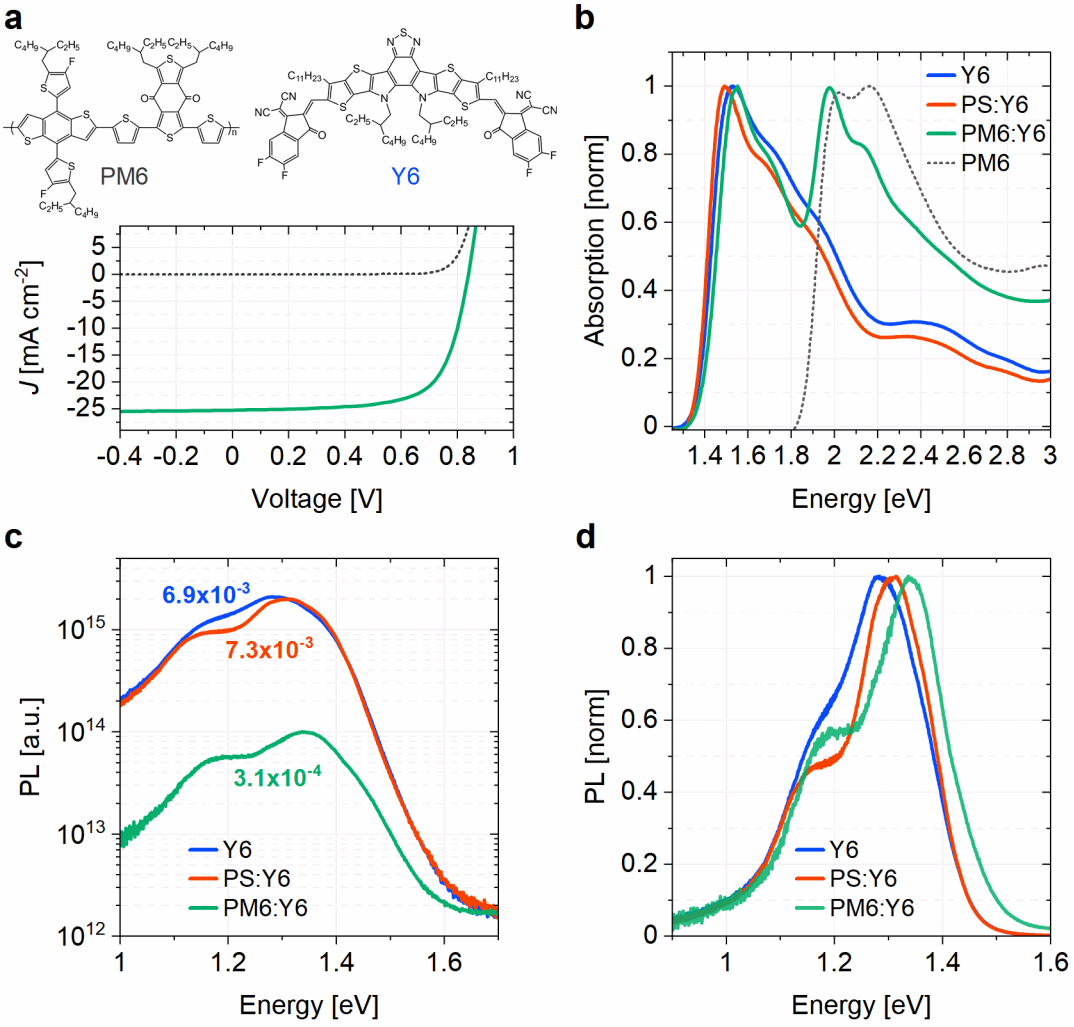

Figure 1: (a) Chemical structure of PM6 and Y6 and the current density-voltage (*JV*) characteristics of a regular device with a 100nm PM6:Y6 active layer measured under simulated AM1.5G light (solid line) and in the dark (dotted line). (b) Normalized absorption spectra of thin films of neat Y6 and blends of PS:Y6 and PM6:Y6 on glass (solid lines) and of neat PM6 on glass (dotted line). (c) Steady-state photoluminescence (PL) spectra of thin films of neat Y6 and blends of PS:Y6 and PM6:Y6 on glass. The values given for each data set correspond to the calculated PLQY value of the samples. (d) Normalized

PL spectra of thin films of neat Y6 and blends of PS:Y6 and PM6:Y6 on glass showing the red-shift of emission peak for neat Y6 and the blend PS:Y6 with respect to the PM6:Y6 film.

As these small spectral changes might be due to orientational and morphological differences and microcavity effects, unambiguous assignment of CT emission and singlet emission is impossible. A way out of this problem is to identify conditions which provide us with the emission from Y6 singlet excitons in the actual multicomponent and multilayer device. We will argue in the following that the later can be gained from PL measurements on complete devices. To this end, we studied the emission and absorption properties of PM6:Y6 single junction devices with different active layer thickness and electrodes (see **Table S1** and **Figure S2**). **Figure 2a** displays the PL spectrum of a device with a semi-transparent back electrode at V_{OC} and under short-circuit (SC) conditions, together with its EL spectrum. We also ensured that the excitation source only illuminates the active area by masking the measured pixel. The excitation intensity in PL is adjusted to generate the same photocurrent density as under simulated AM1.5G excitation, and the same current density was used to drive the device in the EL measurements. We find that the intensity and shape of the PL is virtually the same under V_{OC} and SC conditions. We expect that at SC, all photogenerated free charges are efficiently extracted while open-circuit conditions enforce the recombination of all photogenerated charges. However, the driving conditions have no appreciable effect on the shape of the PL spectrum for a wider bias range and reduce the PL intensity only slightly (see **Figure S3**). A similar observation has been reported recently for another polymer:NFA blend with low energy offset.[22] We conclude that the PL of the PM6:Y6 blend in the device is dominated by the radiative decay of strongly-bound Y6 S_1 excitons and that any radiative emission from states which are reformed upon free charge recombination is hidden under the strong Y6 PL from the initially formed excitons. We also find that the intensity of the PL is ca. 10 times larger than in the EL experiment even though we inject an equivalent number of charges than what was produced during the PL experiment. This indicates that the PL of the blend device comes from incomplete dissociation of Y6 excitons generated far enough from the DA heterojunction, and that the contribution of free carrier recombination to the PL is small to negligible.

Having the Y6 exciton emission spectrum for the BHJ in the device structure at hand, we now turn to the more detailed analysis of the EL spectrum. We find that the EL emission peaks at the same energy and has a similar spectral shape as the PL. There is no indication for the presence of additional strongly-emitting low energy states. Instead, the EL overwhelmingly originates from Y6 singlet excitons formed by free charge recombination either directly or via the CT state manifold. For our semi-transparent device, subtracting the normalized PL from the normalized EL reveals a broad spectrum with a maximum at 1.15 eV, as depicted in **Figure 2b**. In contrast, the PL and EL of a neat Y6 device agree perfectly with one another (**Figure S4**). This implies that the extra emission contribution in the blend EL stems from the radiative

decay of an additional lower lying state, populated in the non-geminate recombination process, probably the CT state. While one may be tempted to analyse this extra emission quantitatively in terms of the energy and spectral width of the CT state manifold, we acknowledge that the spectral shape and strength depends largely on the active layer thickness and device geometry (**see Figure S5**). The stronger the 0-1 (and 0-2) emission peak intensities in the PL, the more pronounced and red-shifted is this extra emission in EL. This points to severe microcavity effects. Optical modelling combined with drift-diffusion simulations would be necessary to analyse these spectra in terms of the intrinsic emission spectrum, which is beyond the scope of this manuscript. Irrespective of these details, the extra low energy contribution accounts to, at maximum, 10 % to the total EL emission intensity, meaning that its ELQY is below $3x10^{-6}$.

Given the small differences between the EL and PL spectral shapes, but the rather large difference in intensity, the question arises whether conclusions from the analysis of the EL spectra are representative of the state population in the active layer under photoexcitation at V_{OC} conditions. For example, the EL efficiency can be easily affected by injection barriers,[23] while the bulk and surface density of photogenerated carriers may be reduced by non-selective contacts.[24] To ensure that both driving conditions create the same free carrier population, we compared the results from steady-state photoinduced absorption (PIA) and electromodulation injection absorption (EMIA) spectroscopy on the very same device. PIA measures the differential absorption upon modulation of the intensity of quasi-steady state illumination while keeping the device at V_{OC}.[25] The method has been recently applied to the PM6:Y6 blend where it was shown that carrier losses due to surface recombination are negligible in regular devices.[26] For our semi-transparent regular device, in **Figure 2c**, the dark squares show the differential absorption at a photon energy of 1.25 eV (assigned to the absorption by the PM6 polaron) as a function of illumination intensity. This is compared to the differential absorption upon modulated dark injection of the same recombination current (the inset figure shows the EMIA spectrum as a function of photon energy at 1 sun equivalent). Above 0.5 equivalent suns, both data sets agree perfectly, meaning that both kinds of excitation create the same carrier densities. Conclusions drawn from EL about the pathways of free carrier recombination are, therefore, representative for the situation under steady state photoexcitation at V_{OC}.

Figure 2d shows the sensitive s-EQE_{PV} spectra of a regular device with a fully reflecting electrode, covering 8 orders of magnitude. This is compared to the S_0-S_1 absorption spectrum as calculated from the PL of the same device (dark grey line) via the optical reciprocity relation: $A(E_\gamma) = \phi_{\mathrm{PL}}(E_\gamma) \times \phi_{\mathrm{BB}}^{-1}(E_\gamma)$ (see solid blue line in **Figure 2d**). The calculated absorption spectrum reproduces all characteristics of the s-EQE_{PV} spectrum, namely the steep incline below 1.4 eV and the weak shoulder at 1.18 eV. Given the proven fact that the PL stems almost exclusively from Y6 exciton emission, we conclude that exciton absorption dominates the entire low energy tail of the s-EQE_{PV}. At very low photon energies ($E_\gamma < 1.05\ eV$) the absorption by trap states becomes apparent.[27] Our data show no evidence for CT-S_1

hybridization at the DA interface, which was predicted to cause an overall red-shift and broadening of the low energy tail of the s-EQE$_{PV}$.[28] We are further able to assign the low energy shoulder in the s-EQE$_{PV}$ spectrum to thermally excited vibronic states of S_0 to the vibronic ground state of S_1, with little to no absorption from CT states or traps. In order to support this conclusion, we measured EQE$_{PV}$ at a lower temperature (see **Figure S6**) and observed that the low energy shoulder is indeed suppressed.

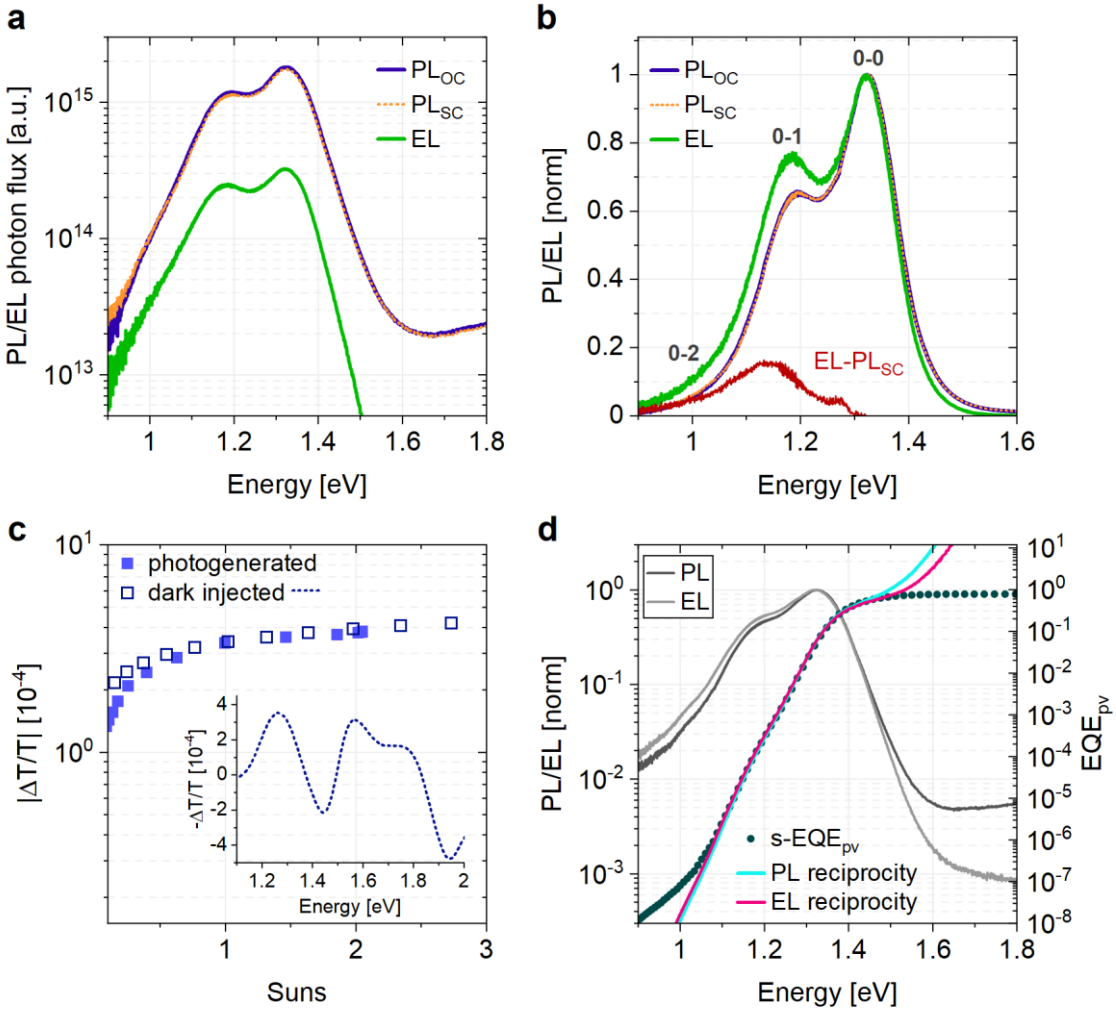

Figure 2: (a) Steady-state photoluminescence (PL) and electroluminescence (EL) spectra of a ca. 135 nm thick regular PM6:Y6 device with semi-transparent cathode. PL was recorded at open-circuit (OC) and short-circuit (SC) conditions under a 1 sun equivalent illumination. In EL, the injected current matched the 1 sun photocurrent density at an applied voltage of 0.90 V. (b) Normalized PL and EL spectra from panel a. The subtraction EL-PL$_{SC}$ reveals a broad emission with a maximum at 1.15 eV (dark red line). (c) Excitation intensity dependent photo-induced absorption spectroscopy (PIA) signals (photogenerated charges, full squares) and electromodulation injection absorption (EMIA) signals (dark injected charges, open squares) measured for a PM6:Y6 regular device with semi-transparent cathode, both at a photon energy of 1.25 eV. The inset figure shows the EMIA spectrum as a function of photon energy at 1 sun equivalent dark injection current. (d) Normalized PL and EL spectra of a ca. 145 nm thick regular PM6:Y6 with fully reflecting electrode (gray lines, left axis). Sensitive photovoltaic

external quantum efficiency (s-EQE$_{PV}$) of the same PM6:Y6 device (dots, right axis). The absorption spectra calculated via the reciprocity relation from the depicted PL and EL are given in blue and pink, respectively.

To conclude this part of the manuscript, we find that the low energy tail of the EQE$_{PV}$ as well as the EL emission spectrum, originating from free charge recombination, are almost entirely determined by the absorption and emission properties of the Y6 singlet exciton. Therefore, these spectra are not suited to draw solid conclusions about the energy and spectral properties of additional low energy states, such as the CT state energy and width. Notwithstanding this, our comparison between the EL and PL spectra and intensity suggest that such states exist and emit at very low quantum efficiency, below 4x10^{-6}. In addition, the data from the above experiments allow us to provide further insight into the role of the Y6 exciton formation and recombination with respect to free charge recombination in the PM6:Y6 blend.

It has been suggested that for a sufficiently low S_1-CT offset, the S_1 is in dynamic equilibrium with the CT state, meaning that the repopulation of the exciton from the CT is faster than its decay to the ground state.[10,22] Also, given that free-carrier recombination in PM6:Y6 is reduced relative to the Langevin-limit,[11,13] it is safe to assume that the CT state occupation is in equilibrium with the free carrier reservoir, as observed for many fullerene and non-fullerene devices. In this case, the chemical potential of the reformed singlet state, μ_{S_1}, is the same as the chemical potential of the CT state, μ_{CT}, this being equal to the quasi-Fermi level splitting, QFLS, of the free charges in the bulk. We determined μ_{S_1} by relating the external photon flux under EL conditions to the excitonic photon emission in the dark: $\phi_{S_1} = \phi_{S_1}^0 \exp\left(\frac{\mu_{S_1}}{k_B T}\right)$ (see the Supporting Information). Here, we remind the reader that we have shown above that dark injection (EL) generates the same carrier density as photoexcitation under the same injection conditions. We determine ϕ_{S_1} by assuming that at least 90 % of the total EL photon flux stems from Y6 exciton recombination. For our 145 nm thick regular device, this yields $\phi_{S_1}(EL) = 6.2 \times 10^{12}\ \mathrm{cm^{-2}s^{-1}}$ (see the Supporting Information for the calculation and **Table S3**). To obtain $\phi_{S_1}^0$, we integrated the optical reciprocity of the device PL (aligned to the tail of the EQE$_{PV}$ spectrum, as shown by the light blue line in **Figure 2d**), yielding $\phi_{S_1}^0 = 0.11\ \mathrm{cm^{-2}s^{-1}}$. This results in $\mu_{S1} = 0.821\ \mathrm{eV}$, which is reasonably close to the measured $V_{\mathrm{OC}} = 0.834\ V$ of the same device and compares well to the QFLS determined for a regular PM6:Y6 device of the same composition via PIA spectroscopy.[26] Thus, we conclude that the population of singlet excitons which are reformed through free charge recombination in this device is indeed in equilibrium with the free carrier reservoir. The analysis of the other devices, with different thicknesses and contacts (see **Table S3**), leads to the same conclusion, though with a bit larger difference between μ_{S_1} and qV_{OC} (30 meV at maximum). While this may indicate that this dynamic equilibrium between singlet excitons and CT states is not always fully established, we also note that the value of

μ_{S1} is determined from the combined results of three different measurements, each with small systematic and statistical errors.

With the knowledge of μ_{S_1}, we can provide an estimate of the population of excited Y6 molecules formed upon free charge carrier encounter via

$$n_{s_1} = N_{S_1} \exp\left(-\frac{E_{S_1}}{k_B T}\right) \exp\left(\frac{\mu_{S_1}}{k_B T}\right) \quad (1a)$$

(note that this equation describes an equilibrated exciton population with $n_{s_1} < N_{S_1}$ for which Boltzmann statistics holds, see the Supporting Information). We determined $E_{S_1} = 1.43\ eV$ from the intersection between the absorption and PL of the blend, as in **Figure S1**. N_{S_1} was set equal to the number density of Y6 molecules in the blend ($N_{Y6} = 2.4 \times 10^{20}\ \mathrm{cm}^{-3}$). With $\mu_{S_1} \cong 0.82$ eV, Eq. 1a yields $n_{s_1} \cong 1.5 \times 10^{10}\ \mathrm{cm}^{-3}$, only. This value is low as compared to the free carrier density and thus hints at a significant barrier for exciton formation from free carrier recombination. To quantify this barrier, we estimated the energy for free electron-hole pairs, E_{CS}, in the limit of an equilibrated non-degenerate carrier population, via[29]

$$n_{CS}^2 = N_{CS}^2 \exp\left(-\frac{E_{CS}}{k_B T}\right) \exp\left(\frac{QFLS}{k_B T}\right) \quad (1b)$$

The free carrier density in PM6:Y6 at 1 sun illumination conditions was reported to be $n_{CS} \approx 2.5 \pm 0.5 \times 10^{16}\ \mathrm{cm}^{-3}$.[11,26] It has also been shown that the QLFS is equal to qV_{OC} for regular devices.[26] Then, with $N_{CS} = N_{Y6}$ and $qV_{OC} \cong 0.83\ eV$ for our 145 nm thick regular device, we obtain $E_{CS} = 1.31 \pm 0.01$ eV (see **Table S3** for the other devices). This results in an $E_{CS} - E_{S_1}$ barrier of 120 meV. To confirm our estimate of this energy offset, we measured the activation energy for exciton formation upon free charge recombination by recording the temperature dependence of the EL intensity for a fixed injection current, keeping the recombination rate constant. As shown in **Figure 3**, decreasing the temperature causes a similar red-shift of the PL and EL spectra (see **Figure S7** for the normalized spectra and the effect of driving conditions), but it only decreases the EL intensity. Interestingly, the temperature does not affect the low energy tail of the EL, supporting our conclusion that it has a different origin than the main emission which is from exciton reformation and decay. Taking the EL peak intensity as a measure for the S_1 population yields an activation energy of 117 ± 4 meV (**Figure 3c**), in very good agreement with the estimate from above. This puts E_{CS} again at around 1.31 eV, as shown schematically in **Figure 4**. Our estimate for E_{CS} challenges recent measurements of the energies of the frontier orbitals of the neat layers and in the blend with cyclophotovoltammetry or photoelectron spectroscopy, which predict values for E_{CS} between 1.0 eV and 1.62 eV.[14,30,31] These conflicting results motivate a comprehensive analysis of the energetics in this blend. Because of the large quadrupole moment of Y6, the frontier orbital offset in the blend may, indeed, differ significantly from the difference between the ionisation energy of the neat donor and the electron affinity of the neat acceptor.[32]

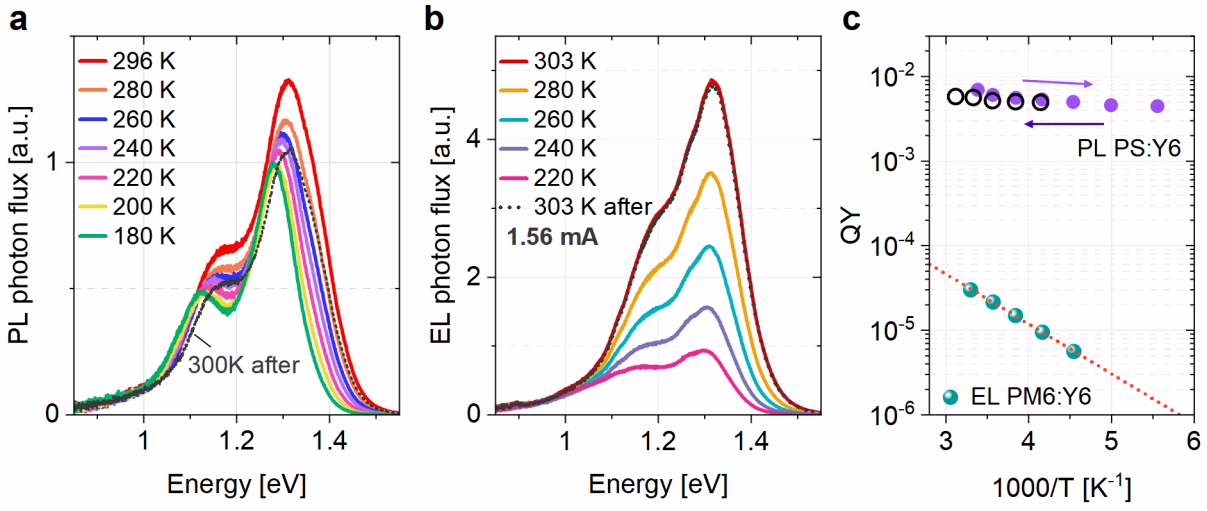

Figure 3: (a) Steady-state photoluminescence (PL) spectra as a function of temperature of a thin film of PS:Y6 on glass. (b) Electroluminescence (EL) spectra as a function of temperature of a regular PM6:Y6 device measured at a constant current of 1.56 mA. (c) Temperature dependence of the PL intensity of a PS:Y6 film and the EL peak intensity of a PM6:Y6 device. The PLQY data was normalized to the value measured at room temperature in the integrating sphere. The full purple dots are the values obtained upon cooling while the open black dots were obtained when heating back up the sample. The ELQY data was normalized to the absolute measurement as well. The red dashed line is a fit to $\mathrm{ELQY} = \exp\left(-\frac{\Delta E}{k_B T}\right)$, which gives an activation energy $\Delta E = 117\ \mathrm{meV}$.

With $E_{S_1} - E_{CS} \cong 120\ \mathrm{meV}$, the PM6:Y6 system is, indeed, a low energy offset blend, though the offset is large enough to ensure efficient dissociation of excitons into free carriers as observed experimentally.[11] It is the reason why this blend generates charges so efficiently. On the other hand, reformation of singlet excitons from free charge generation is rather insignificant. To determine the fraction of charge carrier recombination events proceeding through exciton formation and recombination, we related the ELQY of PM6:Y6 (4×10^{-5}) to the PLQY of the PS:Y6 film (7×10^{-3}), where the latter is the probability that an exciton formed on Y6 emits a photon out. We estimate this fraction to be 0.6 %. All other recombination must proceed via other decay channels, involving state manifolds with very low radiative efficiency, most likely being CT states (see **Figure 4**).

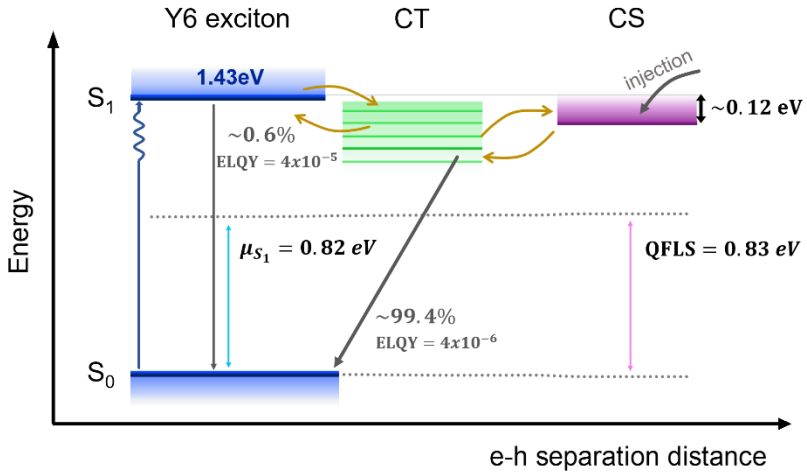

Figure 4: Energy scheme summarizing the main findings of our work. In PM6:Y6 devices, the chemical potential of the Y6 singlet exciton, μ_{S_1}, is almost equal to the QFLS in the bulk, thus singlet excitons are in dynamic equilibrium with free carriers in the CS state, and most likely with the CT state as well. Most of the photon emission of the excited blend originates from the Y6 exciton. However, most non-geminate recombination occurs through a very weakly-emitting state different from the Y6 singlet. We can relate the ELQY of the singlet excitons in the device to the PLQY of the PS:Y6 film, and conclude that less than 0.6 % of injected charges are re-formed into excitons. The low yield of reformation can be explained by the barrier between the singlet energy and the effective transport gap (CS state).

Our results show that the EQE_{PV}, and with that the radiative loss, $\Delta V_{OC,rad}$, is entirely determined by the strongly absorbing Y6 excitons. However, the state manifold through which most recombination proceeds has a much lower absorption strength and is most likely the CT state manifold. Being the dominant decay channel for charge carriers, it is the energetics and kinetics of the CT state which determines the V_{OC} of the PM6:Y6 blend, irrespective of the position and emission properties of the singlet state (see Ref.[33] and the Supporting Information). In fact, in the limit of S_1-CT-CS equilibrium as explained above, the V_{OC} is given by

$$qV_{OC} = E_{CT} + k_B T \ln\left(\frac{J_{SC}}{qd\left(1+\frac{R_{S_1}}{R_{CT}}\right)k_{CT}N_{CT}}\right) \quad (2)$$

where $R_{S_1} = k_{S1}n_{S_1}$ and $R_{CT} = k_{CT}n_{CT}$ are the S_1 and CT recombination rates, respectively, with k_{S_1} and k_{CT} the respective decay coefficients to the ground state. We have shown that $\frac{R_{S_1}}{R_{CT}} < 1\,\%$ in the PM6:Y6 blend, meaning that the properties of the Y6 singlets are almost irrelevant for the V_{OC} of the PM6:Y6 devices, which is instead dominated by the CT population and decay properties. It is only if singlets dominate the total recombination rate that the occupation and energetics of the S_1 state become relevant for the V_{OC}.[33] Unfortunately, reliable information on the CT energetics cannot be gained from the EL and ELQY spectra as

discussed earlier, though we expect an appreciable offset to the S_1 state from the efficient exciton splitting. It is, therefore, instructive to consider the total V_{OC} loss in terms of the energy and recombination properties of free charges. Our analysis puts the charge separated state at ca. 1.31 eV, only 70 meV below the photovoltaic gap of ca. 1.38 eV, which may indeed be the reason for the fairly small open-circuit voltage loss of this blend. The main V_{OC} loss comes from the difference between E_{CS} and the QFLS, which is 0.47 eV. In case of negligible trapping and recombination via low energy states, this difference is given by $E_{CS} - qV_{OC} = \mp k_B T \ln\left(\frac{qdk_2 n_{CS}^2}{J_{SC}}\right)$, where k_2 is the coefficient for non-geminate free charge recombination.[34,35] It was shown recently that the PM6:Y6 blend benefits from a low tail state energetics disorder and exceptionally weak charge trapping.[31] Therefore, the V_{OC} loss originates mainly from a fairly high k_2, which we determined to be $k_2 = (1-2) \times 10^{-11}\mathrm{cm}^3\mathrm{s}^{-1}$.[11] This is only $\cong 50$ times suppressed to the Langevin coefficient for encounter-limited recombination, suggesting additional recombination pathways such as triplet formation or the recombination through midgap-states.[27,36,37] Recent work presented promising concepts to reduce the non-geminate recombination in PM6:Y6-based blends, e.g. through the use of solvent additives,[38] or by employing ternary blends.[39,40]

In conclusion, we find that most non-geminate recombination in PM6:Y6 occurs through a very weakly-emitting (or even dark) low energy state that is different from the Y6 S_1 state from which almost all radiation originates. The chemical potential of the Y6 S_1 state is found to be almost equal to the QFLS in the bulk, meaning that the singlet excitons are in dynamic equilibrium with the free carriers (and most likely with the CT state). This is the exact reason why Rau's reciprocity works so well for PM6:Y6 solar cells. We estimate the singlet energy to lie ca. 120 meV above the effective transport gap, which explains efficient free charge formation and the low yield of exciton reformation. In fact, less than 1 % of the recombination proceeds through exciton reformation and decay. As such, the V_{OC} of the PM6:Y6 blend is almost entirely determined by the energetics and kinetics of the CT state, irrespective of the position and emission properties of the singlet state. It's only when the density and/or the recombination properties of the interfacial CT are substantially reduced that a large gain in V_{OC} can be expected.

Supporting Information

Experimental section, absorption and PL of PM6:Y6 films and EQE_{PV} with its derivative, *PV* parameters, *JV* curves and ELQY of different device configurations, PL at OC and SC conditions and at reverse biases of -1 V, -2V and -3 V, PL and EL of a Y6 neat device, PL vs EL (also normalized) of different device configurations, EQE_{PV} measured at 298 K and 233 K, normalized PL of a PS:Y6 film as a function of temperature and normalized EL of a PM6:Y6 device as a function of temperature, calculation procedure of the chemical potential and photon flux, calculation of the number density of Y6 molecules and calculation of the contribution of the S_1 energetics and recombination properties to V_{OC}, voltage losses and summary of the calculated parameters (emission current, chemical potential and singlet energy-CS barrier) for different device configurations.

Author Information

Corresponding Author:

Dieter Neher – *Institute of Physics and Astronomy, University of Potsdam, Karl-Liebknecht-Str. 24-25, 14476 Potsdam-Golm, Germany*; Email: neher@uni-potsdam.de

Authors:

Lorena Perdigón-Toro – *Institute of Physics and Astronomy, University of Potsdam, Karl-Liebknecht-Str. 24-25, 14476 Potsdam-Golm, Germany*

Le Quang Phuong – *Disordered Semiconductor Optoelectronics, Institute of Physics and Astronomy, University of Potsdam, Karl-Liebknecht-Str. 24-25, 14476 Potsdam-Golm, Germany*

Stefan Zeiske – *Sustainable Advanced Materials (Sêr SAM), Department of Physics, Swansea University, Singleton Park, Swansea, SA2 8PP U.K*

Koen Vandewal – *Instituut voor Materiaalonderzoek (IMO-IMOMEC), Hasselt University, Wetenschapspark 1, BE-3590 Diepenbeek, Belgium*

Ardalan Armin – *Sustainable Advanced Materials (Sêr SAM), Department of Physics, Swansea University, Singleton Park, Swansea, SA2 8PP U.K*

Safa Shoaee – *Disordered Semiconductor Optoelectronics, Institute of Physics and Astronomy, University of Potsdam, Karl-Liebknecht-Str. 24-25, 14476 Potsdam-Golm, Germany*

Acknowledgement

The authors acknowledge the Alexander von Humboldt Foundation for funding. This work was supported by the Sêr Cymru II Program through the Welsh Government, the European

Regional Development Fund, Welsh European Funding Office and Swansea University strategic initiative in Sustainable Advanced Materials. S.Z. is a recipient of a UKRI EPSRC Doctoral Training Partnership studentship and A.A. is a Sêr Cymru II Rising Star Fellow. KV acknowledges funding from the European Research Council (ERC), grant agreement 864625. The authors thank Martin Stolterfoht for long-lived discussions on excitons and their role on PLQY.

References

(1) Liu, Q.; Jiang, Y.; Jin, K.; Qin, J.; Xu, J.; Li, W.; Xiong, J.; Liu, J.; Xiao, Z.; Sun, K.; et al. 18% Efficiency Organic Solar Cells. *Sci. Bull.* **2020**, *65*, 272–275.

(2) Green, M. A.; Dunlop, E. D.; Hohl- Ebinger, J.; Yoshita, M.; Kopidakis, N.; Hao, X. Solar Cell Efficiency Tables (Version 56). *Prog. Photovoltaics Res. Appl.* **2020**, *28*, 629–638.

(3) Meredith, P.; Li, W.; Armin, A. Nonfullerene Acceptors: A Renaissance in Organic Photovoltaics? *Adv. Energy Mater.* **2020**, *10*, 2001788.

(4) Qian, D.; Zheng, Z.; Yao, H.; Tress, W.; Hopper, T. R.; Chen, S.; Li, S.; Liu, J.; Chen, S.; Zhang, J.; et al. Design Rules for Minimizing Voltage Losses in High-Efficiency Organic Solar Cells. *Nat. Mater.* **2018**, *17*, 703–709.

(5) Firdaus, Y.; Le Corre, V. M.; Karuthedath, S.; Liu, W.; Markina, A.; Huang, W.; Chattopadhyay, S.; Nahid, M. M.; Nugraha, M. I.; Lin, Y.; et al. Long-Range Exciton Diffusion in Molecular Non-Fullerene Acceptors. *Nat. Commun.* **2020**, *11*, 1–10.

(6) Hou, J.; Inganäs, O.; Friend, R. H.; Gao, F. Organic Solar Cells Based on Non-Fullerene Acceptors. *Nat. Mater.* **2018**, *17*, 119–128.

(7) Zhang, G.; Chen, X. K.; Xiao, J.; Chow, P. C. Y.; Ren, M.; Kupgan, G.; Jiao, X.; Chan, C. C. S.; Du, X.; Xia, R.; et al. Delocalization of Exciton and Electron Wavefunction in Non-Fullerene Acceptor Molecules Enables Efficient Organic Solar Cells. *Nat. Commun.* **2020**, *11*, 3943.

(8) Azzouzi, M.; Yan, J.; Kirchartz, T.; Liu, K.; Wang, J.; Wu, H.; Nelson, J. Nonradiative Energy Losses in Bulk-Heterojunction Organic Photovoltaics. *Phys. Rev. X* **2018**, *8*, 031055.

(9) Eisner, F. D.; Azzouzi, M.; Fei, Z.; Hou, X.; Anthopoulos, T. D.; Dennis, T. J. S.; Heeney, M.; Nelson, J. Hybridization of Local Exciton and Charge-Transfer States Reduces Nonradiative Voltage Losses in Organic Solar Cells. *J. Am. Chem. Soc.* **2019**, *141*, 6362–6374.

(10) Classen, A.; Chochos, C. L.; Lüer, L.; Gregoriou, V. G.; Wortmann, J.; Osvet, A.; Forberich, K.; McCulloch, I.; Heumüller, T.; Brabec, C. J. The Role of Exciton Lifetime for Charge Generation in Organic Solar Cells at Negligible Energy-Level Offsets. *Nat. Energy* **2020**, *5*, 711–719.

(11) Perdigón-Toro, L.; Zhang, H.; Markina, A.; Yuan, J.; Hosseini, S. M.; Wolff, C. M.; Zuo, G.; Stolterfoht, M.; Zou, Y.; Gao, F.; et al. Barrierless Free Charge Generation in the High-Performance PM6:Y6 Bulk Heterojunction Non-Fullerene Solar Cell. *Adv. Mater.* **2020**, *32*, 1906763.

(12) Zhu, L.; Zhang, M.; Zhou, G.; Hao, T.; Xu, J.; Wang, J.; Qiu, C.; Prine, N.; Ali, J.; Feng, W.; et al. Efficient Organic Solar Cell with 16.88% Efficiency Enabled by Refined

Acceptor Crystallization and Morphology with Improved Charge Transfer and Transport Properties. *Adv. Energy Mater.* **2020**, *10*, 1904234.

(13) Karki, A.; Vollbrecht, J.; Dixon, A. L.; Schopp, N.; Schrock, M.; Reddy, G. N. M.; Nguyen, T. Understanding the High Performance of over 15% Efficiency in Single- Junction Bulk Heterojunction Organic Solar Cells. *Adv. Mater.* **2019**, *31*, 1903868.

(14) Karuthedath, S.; Gorenflot, J.; Firdaus, Y.; Chaturvedi, N.; De Castro, C. S. P.; Harrison, G. T.; Khan, J. I.; Markina, A.; Balawi, A. H.; Peña, T. A. Dela; et al. Intrinsic Efficiency Limits in Low-Bandgap Non-Fullerene Acceptor Organic Solar Cells. *Nat. Mater.* **2020**, 1–7.

(15) Siegmund, B.; Mischok, A.; Benduhn, J.; Zeika, O.; Ullbrich, S.; Nehm, F.; Böhm, M.; Spoltore, D.; Fröb, H.; Körner, C.; et al. Organic Narrowband Near-Infrared Photodetectors Based on Intermolecular Charge-Transfer Absorption. *Nat. Commun.* **2017**, *8*, 1–6.

(16) List, M.; Sarkar, T.; Perkhun, P.; Ackermann, J.; Luo, C.; Würfel, U. Correct Determination of Charge Transfer State Energy from Luminescence Spectra in Organic Solar Cells. *Nat. Commun.* **2018**, *9*, 1–8.

(17) Armin, A.; Zarrabi, N.; Sandberg, O. J.; Kaiser, C.; Zeiske, S.; Li, W.; Meredith, P. Limitations of Charge Transfer State Parameterization Using Photovoltaic External Quantum Efficiency. *Adv. Energy Mater.* **2020**, *10*, 2001828.

(18) Rau, U. Reciprocity Relation between Photovoltaic Quantum Efficiency and Electroluminescent Emission of Solar Cells. *Phys. Rev. B - Condens. Matter Mater. Phys.* **2007**, *76*, 085303.

(19) Ullbrich, S.; Benduhn, J.; Jia, X.; Nikolis, V. C.; Tvingstedt, K.; Piersimoni, F.; Roland, S.; Liu, Y.; Wu, J.; Fischer, A.; et al. Emissive and Charge-Generating Donor–Acceptor Interfaces for Organic Optoelectronics with Low Voltage Losses. *Nat. Mater.* **2019**, *18*, 459–464.

(20) Vandewal, K.; Mertens, S.; Benduhn, J.; Liu, Q. The Cost of Converting Excitons into Free Charge Carriers in Organic Solar Cells. *J. Phys. Chem. Lett.* **2019**, *11*, 129–135.

(21) Zou, X.; Wen, G.; Hu, R.; Dong, G.; Zhang, C.; Zhang, W.; Huang, H.; Dang, W. An Insight into the Excitation States of Small Molecular Semiconductor Y6. *Molecules* **2020**, *25*, 4118.

(22) Hinrichsen, T. F.; Chan, C. C. S.; Ma, C.; Paleček, D.; Gillett, A.; Chen, S.; Zou, X.; Zhang, G.; Yip, H. L.; Wong, K. S.; et al. Long-Lived and Disorder-Free Charge Transfer States Enable Endothermic Charge Separation in Efficient Non-Fullerene Organic Solar Cells. *Nat. Commun.* **2020**, *11*, 1–10.

(23) Gu, Y.; Liu, Y.; Russell, T. P. Fullerene- Based Interlayers for Breaking Energy Barriers in Organic Solar Cells. *Chempluschem* **2020**, *85*, 751–759.

(24) Spies, A.; List, M.; Sarkar, T.; Würfel, U. On the Impact of Contact Selectivity and Charge Transport on the Open-Circuit Voltage of Organic Solar Cells. *Adv. Energy Mater.* **2017**, *7*, 1601750.

(25) Quang Phuong, L.; Mehrdad Hosseini, S.; Woo Koh, C.; Young Woo, H.; Shoaee, S. Measuring Competing Recombination Losses in a Significantly Reduced Langevin System by Steady-State Photoinduced Absorption and Photocurrent Spectroscopy. *J. Phys. Chem. C* **2019**, *123*, 27417–27422.

(26) Phuong, L. Q.; Hosseini, S. M.; Sandberg, O. J.; Zou, Y.; Woo, H. Y.; Neher, D.; Shoaee, S. Quantifying Quasi-Fermi Level Splitting and Open-Circuit Voltage Losses in Highly Efficient Nonfullerene Organic Solar Cells. *Sol. RRL* **2020**, 2000649.

(27) Zarrabi, N.; Sandberg, O. J.; Zeiske, S.; Li, W.; Riley, D. B.; Meredith, P.; Armin, A. Charge-Generating Mid-Gap Trap States Define the Thermodynamic Limit of Organic Photovoltaic Devices. *Nat. Commun.* **2020**, *11*, 1–10.

(28) Chen, X.-K.; Coropceanu, V.; Brédas, J.-L. Assessing the Nature of the Charge-Transfer Electronic States in Organic Solar Cells. *Nat. Commun.* **2018**, *9*, 5295.

(29) Würfel, P. *Physics of Solar Cells : From Principles to New Concepts*; Wiley-VCH, 2005.

(30) Yuan, J.; Zhang, Y.; Zhou, L.; Zhang, G.; Yip, H.-L.; Lau, T.-K.; Lu, X.; Zhu, C.; Peng, H.; Johnson, P. A.; et al. Single-Junction Organic Solar Cell with over 15% Efficiency Using Fused-Ring Acceptor with Electron-Deficient Core. *Joule* **2019**, *3*, 1140–1151.

(31) Wu, J.; Lee, J.; Chin, Y. C.; Yao, H.; Cha, H.; Luke, J.; Hou, J.; Kim, J. S.; Durrant, J. R. Exceptionally Low Charge Trapping Enables Highly Efficient Organic Bulk Heterojunction Solar Cells. *Energy Environ. Sci.* **2020**, *13*, 2422–2430.

(32) Schwarze, M.; Tress, W.; Beyer, B.; Gao, F.; Scholz, R.; Poelking, C.; Ortstein, K.; Günther, A. A.; Kasemann, D.; Andrienko, D.; et al. Band Structure Engineering in Organic Semiconductors. *Science* **2016**, *352*, 1446–1449.

(33) Linderl, T.; Hörmann, U.; Beratz, S.; Gruber, M.; Grob, S.; Hofmann, A.; Brütting, W. Temperature Dependent Competition between Different Recombination Channels in Organic Heterojunction Solar Cells. *J. Opt. (United Kingdom)* **2016**, *18*, 024007.

(34) Blakesley, J. C.; Neher, D. Relationship between Energetic Disorder and Open-Circuit Voltage in Bulk Heterojunction Organic Solar Cells. *Phys. Rev. B* **2011**, *84*, 075210.

(35) Collins, S. D.; Proctor, C. M.; Ran, N. A.; Nguyen, T.-Q. Understanding Open-Circuit Voltage Loss through the Density of States in Organic Bulk Heterojunction Solar Cells. *Adv. Energy Mater.* **2016**, *6*, 1501721.

(36) Shoaee, S.; Armin, A.; Stolterfoht, M.; Hosseini, S. M.; Kurpiers, J.; Neher, D. Decoding Charge Recombination through Charge Generation in Organic Solar Cells. *Sol. RRL* **2019**, *3*, 1900184.

(37) Gillett, A. J.; Privitera, A.; Dilmurat, R.; Karki, A.; Qian, D.; Pershin, A.; Londi, G.; Myers, W. K.; Lee, J.; Yuan, J.; et al. The Role of Charge Recombination to Spin-Triplet Excitons in Non-Fullerene Acceptor Organic Solar Cells. **2020**.

(38) Hosseini, S. M.; Tokmoldin, N.; Lee, Y. W.; Zou, Y.; Woo, H. Y.; Neher, D.; Shoaee, S. Putting Order into PM6:Y6 Solar Cells to Reduce the Langevin Recombination in 400 Nm Thick Junction. *Sol. RRL* **2020**, *4*, 2000498.

(39) Yan, T.; Song, W.; Huang, J.; Peng, R.; Huang, L.; Ge, Z. 16.67% Rigid and 14.06% Flexible Organic Solar Cells Enabled by Ternary Heterojunction Strategy. *Adv. Mater.* **2019**, *31*, 1902210.

(40) Gasparini, N.; Paleti, S. H. K.; Bertrandie, J.; Cai, G.; Zhang, G.; Wadsworth, A.; Lu, X.; Yip, H.-L.; McCulloch, I.; Baran, D. Exploiting Ternary Blends for Improved Photostability in High-Efficiency Organic Solar Cells. *ACS Energy Lett.* **2020**, *5*, 1371–1379.